Adaptive sliding mode control of interleaved parallel boost converter for fuel cell energy generation system

El Fadil, H.; Giri, F. ; Guerrero, Josep M.

Published in:
Mathematics and Computers in Simulation

DOI (link to publication from Publisher):
10.1016/j.matcom.2012.07.011

Publication date:
2013

Document Version
Early version, also known as pre-print

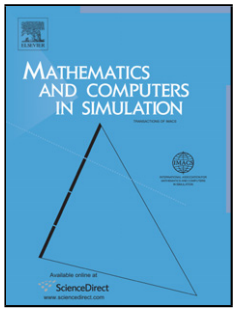

Title: Adaptive sliding mode control of interleaved parallel boost converter for fuel cell energy generation system

Authors: H. El Fadil, F. Giri, J.M. Guerrero

PII: S0378-4754(12)00174-7
DOI: doi:10.1016/j.matcom.2012.07.011
Reference: MATCOM 3831

To appear in: *Mathematics and Computers in Simulation*

Received date: 25-10-2011
Revised date: 8-5-2012
Accepted date: 1-7-2012

Please cite this article as: H.E. Fadil, F. Giri, J.M. Guerrero, Adaptive sliding mode control of interleaved parallel boost converter for fuel cell energy generation system, *Mathematics and Computers in Simulation* (2010), doi:10.1016/j.matcom.2012.07.011

Adaptive sliding mode control of interleaved parallel boost converter for fuel cell energy generation system

H. El Fadil[1*], F. Giri[1], J.M. Guerrero[2]

1. GREYC Lab, Université de Caen Basse-Normandie, UMR 6072, 14032 Caen, France.
(E-mails: elfadilhassan@yahoo.fr , fouad.giri@unicaen.fr ; * Corresponding Author)

2. Institute of Energy Technology, Aalborg University, Aalborg East DK-9220, Denmark (e-mail: joz@et.aau.dk).

Abstract - This paper deals with the problem of controlling energy generation systems including fuel cells (FCs) and interleaved boost power converters. The proposed nonlinear adaptive controller is designed using sliding mode control (SMC) technique based on the system nonlinear model. The latter accounts for the boost converter large-signal dynamics as well as for the fuel-cell nonlinear characteristics. The adaptive nonlinear controller involves online estimation of the DC bus impedance 'seen' by the converter. The control objective is threefold: (i) asymptotic stability of the closed loop system, (ii) output voltage regulation under bus impedance uncertainties and (iii) equal current sharing between modules. It is formally shown, using theoretical analysis and simulations, that the developed adaptive controller actually meets its control objectives.

Keywords – Fuel cell, interleaved boost converter, sliding mode control, adaptive control.

1. Introduction

It is well established that the past-decades intensive use of fossil fuel has already caused global environmental problems. Furthermore, the gap between fossil fuel resources and the global energy demand has been growing over the few past years leading to significant oil price increase. More recently, the Fukushima disaster has showed the drawbacks of using nuclear energy as alternative to fossil fuel. On the other hand, renewable energy has gained in popularity, since their efficiency is continuously improved and their cost is continuously reduced. Indeed, renewable energy systems produce electric power without polluting the environment, transforming free inexhaustible energy resources, like solar radiation or wind,

into electricity. The world's demand for electrical energy has been continuously increasing and is expected to continue growing, while the majority of the electrical energy in most countries is generated by conventional energy sources. The ongoing global climate change, the diminution of fossil fuel resources and the collective fear of energy supply shortage have made the global energy trends more complex. However, it is disadvantageous to meet the rising electricity demand by establishing more conventional power systems. As the electricity is delivered from the main power plants to the end-users (customers) at a high voltage level along with long length transmission lines, the end-users get short of electricity whenever the lines are destroyed by unexpected events (e.g. natural disasters) or when fuel suppliers fail. Therefore, the penetration of distributed generation (DG) (see Fig.1) at medium and low voltages is expected to play a main role in future power systems.

Implementing distributed energy resources (DER) such as wind turbines, photovoltaic (PV), gas turbines and fuel cells into interconnected grids could be part of the solution to the rising electricity demand problem [1,21]. DG technologies are currently being investigated and developed in many research projects to perform smart grids. On the other hand, mini-grids including DG are installed into rural areas of developing countries. As rural settlements in these countries are scattered, power systems in these areas depend on available energy sources. This involves various issues such as power system control, energy management and load dispatch.

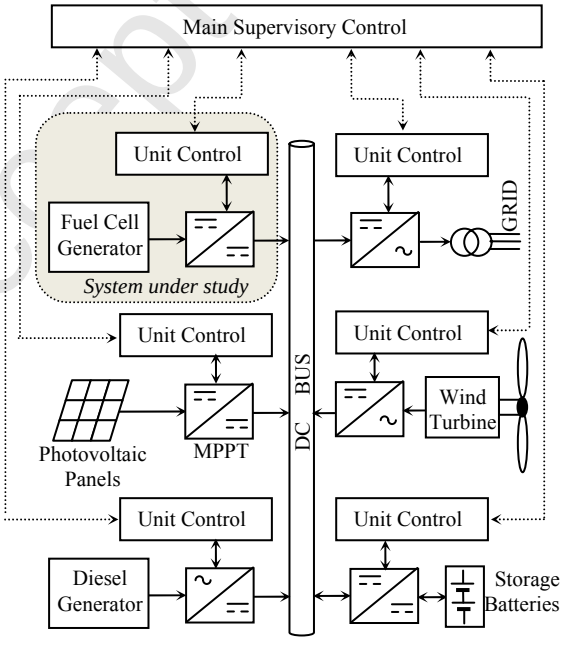

Fig.1: DC microgrid example in distributed energy resources.

Among renewable energies, hydrogen and fuel cell are considered as promising alternatives from both energy storage and supply reliability viewpoints. Indeed, these sources do not only feature a high-efficiency chemical-energy conversion (into electrical energy) but also feature low emissions [24,25,26].

The proliferation of DC-ended sources like PV, batteries, supercapacitors and FCs has made it possible to conceive DC distribution systems or DC microgrids which are main tools for energy sources integration. As the various types of sources have different characteristics, it is important to make sure that each source comes into operation only when ambient conditions (wind, radiation…) are favourable. In this respect, it is well known that FCs does not well bear sudden current variations (current derivative is limited). This is coped with by including bidirectional energy modules (e.g. batteries, supercapacitors) in DERs. Doing so, sudden current variations are supported by the rapid sources. The repartition of the global current generation effort on the different sources of a DER is managed by the main supervisory control (MSC) (Fig. 1). Specifically, when a sudden current demand is detected in the DC bus, the MSC acts on one (or more) rapid source converter changing its direction to discharging mode so that is provides the extra current.

It turns out that, in DERs, different power converters (between sources and DC bus) are involved. In this paper, the focus is made on the integration of fuel cell, through interleaved boost converter (IBC), into a DC microgrid (Fig.1). The IBC topology consists of a number of paralleled boost converters controlled by means of interleaving control techniques in contrast to the conventional high power boost converter [33]. The aim is to control the FC-IBC association so that the integration to the microgrid is accomplished complying with interconnection conventions. In particular, the DC link voltage must be tightly regulated. IBCs offer many benefits making them particularly suitable in different renewable energy applications, e.g. battery chargers and maximum power point tracking (MPPT) in PV conversion. Indeed, they offer good efficiency and voltage/current ripples reduction [20,31]. In this respect, recall that FCs are vulnerable to current ripples making inappropriate the association with more basic converters, particularly boost converters which are known to inject current ripples [32]. Using interleaving techniques, the ripples of corresponding inductor currents and capacitor voltage are diminished, making possible size reduction of inductors and capacitor [27,6]. Moreover, the power losses in IBCs are reduced (compared to basic boost converters) because the switching frequency can be made smaller by increasing the number of branches. Energetic efficiency can also be improved by considering variants of the IBC topology, e.g. soft switching and resonant techniques, or coupled inductors [27].

On the other hand, the research in the fuel cell field has gained more importance and industry applications range from low power (50W) to high power (more than 250kW) [15]. In order to obtain efficient fuel cell systems, the DC/DC converter should be properly designed [3,12,14]).

The above mentioned benefits makes IBCs good candidate for interfacing fuel cell and DC buses [10,19]. The control of IBC topology has been dealt with using conventional linear control techniques [2,11,23,26,29]. The point is that, both the IBC converter and the fuel cell exhibit highly nonlinear behavior making linear controllers only effective within around specific operation points. In this paper, the problem of controlling fuel cell IBC systems is dealt with based on a more accurate model that really accounts for the system nonlinearities. Doing so, the model turns out to be well representative of both the boost converter large-signal dynamic behavior and the fuel-cell nonlinear characteristics. A nonlinear adaptive controller is designed, using the sliding mode control (SMC) technique, to achieve three objectives: (i) asymptotic stability of the closed loop system; (ii) tight output DC link voltage regulation, despite bus impedance uncertainties; (iii) and equal current sharing between modules. Accordingly, the controller involves online estimation of the DC bus impedance 'seen' by the converter. It is formally shown, using theoretical analysis and simulations, that the developed adaptive controller actually meets its control objectives.

The paper is organized as follows. In Section 2, the IBC for fuel cell applications are described and modeled. Section 3 is devoted to the controller design and closed-loop theoretical analysis. The controller tracking performances are illustrated through numerical simulations in Section 4. Section 5 provides the conclusion of the paper.

2. General norms and system modeling

Figure 2 shows the power stage of a fuel cell interleaved boost converter (FC-IBC) system. It consists of a FC generator and N-interleaved boost converters connected in parallel sharing a common DC bus. Each boost converter consisted of an input inductor L_k, a static switch (S_k) controlled by the binary input signal u_k, and an output diode D_k (k =1,…, N). Each diode cathode is connected to the same point with the output capacitor C in parallel with the load represented by a pure resistance R, according to the input impedance of the DC bus. This impedance is actually unknown because it depends on the power demand. This uncertainty will be investigated in next section.

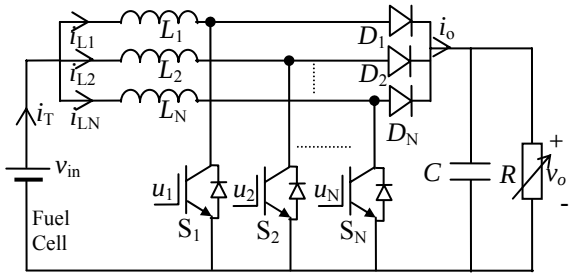

Fig.2: Power stage of the FC-IBC system

2.1. Fuel cell V-I static characteristic

The static V-I polarization curve for a single-cell fuel cell is shown in Fig. 3, where the drop of the fuel cell voltage with load current density can be observed. This voltage reduction is caused by three major losses [13]: activation losses, ohmic losses, and transport losses. The *V-I* polarization curve of Fig.3 corresponds to a Ballard manufacturer elementary FC 1020ACS. The fuel cell used in this application is a proton exchange membrane (PEM), being the operation temperature relatively low. As can be seen from Fig. 3 there is a big difference between the minimum and maximum voltage of the FC generator. Then, it is very important to take into account the nonlinearity of this characteristic for control design purposes. With this aim, a polynomial approximation of the V-I curve of Fig.3 is obtained by using the *polyfit* function of MATLAB defined as follows:

$$v_{in} = \sum_{n=0}^{7} p_n (i_T)^n \overset{def}{=} \varphi(i_T) \tag{1}$$

where $p_n\,(n = 0,...,7)$ are the coefficients listed in Table 1.

Table 1: polynomial coefficients

$p_0 = 10^3$	$p_1 = -35.9$	$p_2 = 2.45$
$p_3 = -0.09$	$p_4 = 1.8\text{x}10^{-3}$	$p_5 = -2\text{x}10^5$
$p_6 = 1.14\text{x}10^{-7}$	$p_7 = -2.64\text{x}10^{-10}$	

Figure 4 shows that the polynomial approximation fits perfectly the real V-I curve. Thus, the approximated function (1) will be used for the control design, which will be addressed in section 3.

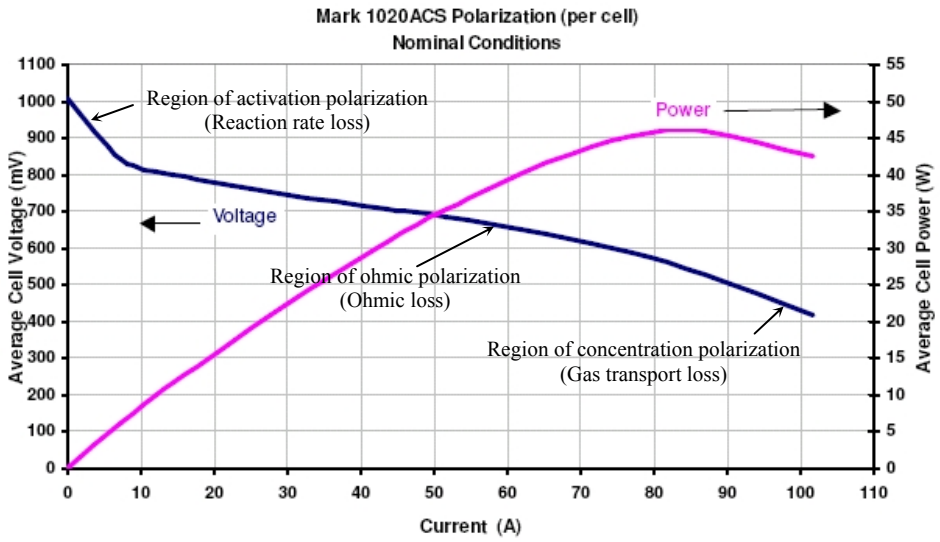

Fig.3: V-I characteristic of elementary single cell of the Fuel Cell 1020ACS made by Ballard.

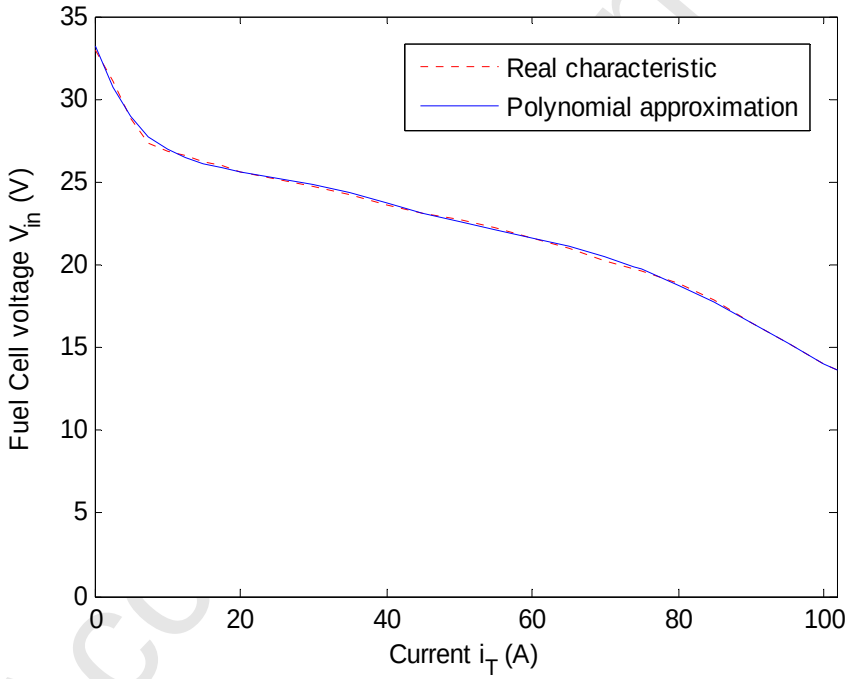

Fig.4: FC V-I characteristic and its polynomial approximation

2.2. Interleaved boost converter modeling

The aim of this subsection is to obtain a large-signal model of the IBC topology taking into account their nonlinearities, which will be useful for the control design procedure. From Fig. 2 one can obtain the power stage bilinear equations, considering some non-idealities. For instance, each inductance of the IBC shown in Fig.2 $L_k\,(k=1,\ldots,N)$ presents an equivalent series resistance (ESR): r_{Lk}. Each k^{th} single boost converter stage is controlled by using

interleaved PWM signal u_k which takes values from the subset $\{0,1\}$. For simplicity, one can consider identical inductances, being:

$$\begin{cases} L_1 \cong L_2 \cong .... \cong L_N \cong L \\ r_{L1} \cong r_{L2} \cong .... \cong r_{LN} \cong r_L \end{cases} \tag{2}$$

From inspection of the circuit, shown in Fig.2, and taking into account that u_k can take the binary values 1 or 0, the following bilinear switching model can be obtained:

$$\frac{di_{Lk}}{dt} = -(1-u_k)\frac{v_o}{L} - \frac{r_L}{L} i_{Lk} + \frac{\varphi(i_T)}{L} \tag{3a}$$

$$\frac{dv_o}{dt} = \frac{1}{C} i_T - \frac{1}{RC} v_0 - \frac{1}{C}\sum_{j=1}^{N} u_j i_{Lj} \tag{3b}$$

where

$$i_T = \sum_{k=1}^{N} i_{Lk} \tag{3c}$$

being N the number of the IBCs connected in parallel. This model is useful for circuit simulation purposes but not for the controller design, because it involves a number of N binary control inputs u_k. For control design purpose, it is more convenient to consider the following averaged model [17], obtained by averaging the model (3) over one switching period T_s ($\bar{x} =< x >= \frac{1}{T_s}\int_0^{T_s} x(t)dt$)

$$\dot{x}_{1k} = -(1-\mu_k)\frac{1}{L} x_2 - \frac{r_L}{L} x_{1k} + \frac{\varphi(x_T)}{L} \tag{4a}$$

$$\dot{x}_2 = \frac{1}{C} x_T - \frac{1}{RC} x_2 - \frac{1}{C}\sum_{j=1}^{N} \mu_j x_{1j} \tag{4b}$$

$$x_T = \sum_{k=1}^{N} x_{1k} \tag{4c}$$

being x_{1k} the average value of the current i_{Lk} ($x_{1k} =< i_{Lk} >$), x_2 is the average value of the

output voltage v_o ($x_2 =< v_o >$), x_T is the average value of the input current i_T ($x_T =< i_T >$), and μ_k is the duty cycle, i.e. average value of the binary control input u_k ,($\mu_k =< u_k >$) which takes values in [0,1].

Notice that the model (4) is a multi-input multi-output (MIMO) system, which can be difficult to control by using classical linear control theory.

3. Adaptive control design

With the aim of design an appropriate control for the nonlinear model (4) described in previous section, the control objectives and the control design is proposed in this Section taking into account the nonlinearities and the uncertainty of the load.

3.1. Control objectives

In order to define the control strategy, first one has to establish the control objectives, which can be formulated as following:

(i) Output voltage regulation under load uncertainty. This is necessary to maintain the voltage constant in the DC bus, avoiding load damages.

(ii) Equal current sharing between modules. The input current waveforms should be equal in order to avoid overloading one of the modules, especially when supplying heavy loads. Also the currents must be interleaved in order to reduce the current ripple which is undesirable in fuel cells.

(iii) Asymptotic stability of the closed loop system. Global asymptotic stability is required to avoid imposing restrictions on the allowed initial conditions.

3.2. Adaptive sliding mode controller (SMC) design

Once the control objectives are defined, as the MIMO system is highly nonlinear, an adaptive sliding mode control is proposed here due to its robustness against uncertainties and parametric estimation capability [28,30].

One of the uncertainties is the load resistance *R* of the model (4), which may be subject to step changes. These load steps occur when the power in the DC bus varies accordingly to the active power of the loads to be supplied. To cope with such a model uncertainty, the controller will be given a more flexible and adaptive capability. More specifically, the controller to be designed should include an on-line estimation of the unknown parameter

$$\frac{1}{R} = \theta \tag{5}$$

The corresponding estimate is denoted $\hat{\theta}$, and the parameter estimation error is

$$\tilde{\theta} = \theta - \hat{\theta}. \tag{6}$$

Moreover, the controller may take into account the nonlinearity of the fuel cell characteristic represented by (1).

The control objective is to enforce the output voltage to track a given constant reference signal V_d despite the system parameter uncertainties. However, it is well known that the boost converter has a non-minimum phase feature (see e.g. [4,5,8,9]). Such an issue is generally dealt by resorting to an indirect design strategy. More specifically, the objective is to enforce the current i_T to track a reference signal, named x_{Td}. The latter is chosen so that if in steady state $i_T = x_{Td}$, then $v_o = V_d$, where $V_d > \min(\varphi(i_T)$ which denotes the desired output voltage. It is derived from the power conservation consideration, also named PIPO, i.e. power input equal to power output, that x_{Td} depends on V_d through the following relationship

$$x_{Td} = \frac{V_d^2}{\left(R\varphi(x_{Td})\right)} \overset{def}{=} \frac{V_d^2}{\varphi(x_{Td})}\theta. \tag{7}$$

This equation shows that the reference current signal x_{Td} depends on the uncertainty, which does not usually appear in the standard adaptive control theory (see e.g. [18]). The objective here is that the current i_T tracks the estimated reference signal $\hat{x}_{Td}$, which is defined as follows

$$\hat{x}_{Td} = \frac{V_d^2}{\varphi(\hat{x}_{Td})}\hat{\theta}. \tag{8}$$

In order to carry out the tracking objective despite the system parameter uncertainties SMC will be used [30]. As already mentioned, the way this technique is applied is not usual because the reference trajectory depends on the estimating of the unknown system parameter $\hat{\theta}$. Keeping in mind the current sharing objective, the following sliding surface is introduced

$$s_k(x) = x_{1k} - \hat{I}_d \tag{9}$$

where

$$\hat{I}_d = \frac{\hat{x}_{Td}}{N} = \frac{V_d^2}{N\varphi(\hat{x}_{Td})}\hat{\theta}. \tag{10}$$

The control objective is to enforce the system state to reach the sliding surface $S_k = 0$. When such a purpose is achieved, the system is said to be in a sliding mode. In that case, we have the so-called invariant condition [30]

$$s_k = \dot{s}_k = 0. \tag{11}$$

The equivalent control can easily be obtained by using (11), (9), (10), and (4a), as follows

$$\mu_{keq} = 1 + \frac{1}{x_2}\left(r_L x_{1k} - \varphi(x_T) + L\dot{\hat{I}}_d \right) \tag{12}$$

From this equation, we can decompose the general control structure as follows

$$\mu_k = \mu_{keq} + \mu_{kN} - \frac{L}{x_2} k_1 \varepsilon_{2k} \tag{13}$$

where $k_1 > 0$ is a design parameter and

$$\mu_{kN} = \frac{L}{x_2}\hat{\mu}_{kN} \tag{14}$$

where $\hat{\mu}_{kN}$ is as yet an additional input, and

$$\varepsilon_{2k} = x_2 - x_{2dk} \tag{15}$$

is the error between the output voltage x_2 and its desired value x_{2dk} for the k^{th} module. The desired value x_{2dk} will be specified later. In (13) the term $k_1\varepsilon_{2k}$ is a damping term introduced in the control law to modify the output response. The objective of SMC is to force the system states to satisfy $s_k = 0$. To this end, one must ensure that the system is capable of reaching the

state $s_k = \dot{s}_k = 0$ from any initial conditions and, having reached $s_k = 0$, that the control action is capable of maintaining the system at $s_k = 0$. Furthermore, the parameter update law and the control law must be chosen in order to stabilize the whole system with state vector is ($s, \varepsilon_2, \tilde{\theta}$). These conditions may be satisfied by considering the quadratic Lyapunov function of the form

$$V = \frac{1}{2} s^T s + \frac{1}{2} \varepsilon_2^T \varepsilon_2 + \frac{1}{2\gamma} \tilde{\theta}^2 \tag{16}$$

where

$$s = [s_1, ..., s_N]^T, \ \varepsilon_2 = [\varepsilon_{21}, ..., \varepsilon_{2N}]^T \tag{17}$$

being $\gamma > 0$ a real constant, called parameter adaptation gain [28]. Our goal is to make the time derivative of V, $\dot{V}$, non-positive definite. Thus $\dot{V}$ is obtained by using (4a) and (9), which yields to

$$\dot{V} = \frac{1}{L} \sum_{k=1}^{N} s_k \left(-(1-\mu_k) x_2 - r_L x_{1k} + \varphi(x_T) - L \dot{\hat{I}}_d \right) + \sum_{k=1}^{N} \varepsilon_{2k} \dot{\varepsilon}_{2k} - \frac{1}{\gamma} \tilde{\theta} \dot{\hat{\theta}} \tag{18}$$

because $\dot{\tilde{\theta}} = -\dot{\hat{\theta}}$ (the uncertain parameter θ is supposed to be subject to non-periodic step changes). By using (12), (13) and (14), Equation (18) takes the form

$$\dot{V} = \sum_{k=1}^{N} s_k \hat{\mu}_{kN} - k_2 \sum_{k=1}^{N} \varepsilon_{2k}^2 - \tilde{\theta} \left(\frac{\dot{\hat{\theta}}}{\gamma} + \frac{x_2}{C} \sum_{k=1}^{N} \varepsilon_{2k} \right) + \sum_{k=1}^{N} \varepsilon_{2k} \left(\dot{\varepsilon}_{2k} - k_1 s_k + k_2 \varepsilon_{2k} + \frac{x_2}{C} \tilde{\theta} \right) \tag{19}$$

where $k_2 > 0$ is the second design parameter. Equation (19) clearly shows that the stability of the closed loop system with the state vector ($s, \varepsilon_2, \tilde{\theta}$) is achieved by simply choosing $\hat{\mu}_N$, $\dot{\varepsilon}_{2k}$, and $\dot{\hat{\theta}}$ so that

$$\hat{\mu}_{kN} = -\alpha \, \mathrm{sgn}(s_k) \tag{20a}$$

$$\dot{\varepsilon}_{2k} - k_1 s_k + k_2 \varepsilon_{2k} + \frac{x_2}{C} \tilde{\theta} = 0 \tag{20b}$$

$$\frac{\dot{\hat{\theta}}}{\gamma}+\frac{x_2}{C}\sum_{k=1}^{N}\varepsilon_{2k}=0 \tag{20c}$$

where $\alpha>0$ is a design parameter and sgn(·) is the sign function. From (20c) the adaptive control law is derived as follows

$$\dot{\hat{\theta}}=-\frac{\gamma}{C}x_2\sum_{k=1}^{N}\varepsilon_{2k}\ . \tag{21}$$

The time derivative of $\hat{I}_d$, is obtained by using (10) and (21), yielding

$$\dot{\hat{I}}_d=-\beta x_2\sum_{k=1}^{N}\varepsilon_{2k} \tag{22}$$

where

$$\beta=\frac{V_d^2\gamma}{\left(N\varphi(\hat{x}_{Td})+NV_d^2\hat{\theta}\dfrac{\phi(\hat{x}_{Td})}{\varphi(\hat{x}_{Td})}\right)C} \tag{23a}$$

where

$$\phi(\hat{x}_{Td})=\left.\frac{d\varphi(x)}{dx}\right|_{x=\hat{x}_{Td}} \tag{23b}$$

Combining equations (13), (12), (14) and (20a), yields the following control law

$$\mu_k=1+\frac{L}{x_2}\left(\frac{r_L}{L}x_{1k}-\alpha\,\mathrm{sgn}(s_k)-k_1(x_2-x_{2dk})-\frac{\varphi(x_T)}{L}-\beta x_2\sum_{j=1}^{N}\varepsilon_{2j}\right) \tag{24}$$

where the dynamic of x_{2dk} is defined, using (4b), (5), (6), (15), and (20b), by the following differential equation:

$$\dot{x}_{2dk}=-k_1 s_k+k_2(x_2-x_{2dk})+\frac{x_T}{C}-\frac{\hat{\theta}}{C}x_2-\frac{1}{C}\sum_{j=1}\mu_j x_{1j} \tag{25a}$$

The resulting closed-loop system is analysed in the following Theorem.

Theorem 1: Consider the closed-loop system consisting of a fuel cell interleaved boost

converter system represented by (4a-b) subject to uncertain load resistor R, and the controller composed of the adaptive control law (24) the parameter update law (21) and dynamic of the desired trajectory x_{2d} of the output voltage (25). Then, one has: (i) the closed-loop system is globally asymptotically stable; (ii) the sliding surfaces s_k converge to zero, this propriety ensures the proper current sharing between modules; and (iii) the estimation error $\tilde{\theta} = \theta - \hat{\theta}$ converges to zero which means that the estimated reference current $\hat{x}_{Td}$ converge to its real value x_{Td}, hence the tracking error $\varepsilon = x_2 - V_d$ converges to zero, this propriety ensures tight regulation under uncertainties □

Remark 1. Adding $k_2 x_{2dk}$ to both sides of (25a) and operating on both sides of the resulting equation by $1/(s+k_2)$, yields:

$$x_{2dk} = \frac{1}{s+k_2}\left[-k_1 s_k + k_2 x_2 + \frac{x_T}{C} - \frac{\hat{\theta}}{C}x_2 - \frac{1}{C}\sum_{j=1}\mu_j x_{1j}\right] \tag{25b}$$

Note that the 1st order transfer function $1/(s+k_2)$ is physically realizable because it is strictly proper and all signals on the right side of (25b) are available. Therefore, the expression (25b) can be practically implemented to online compute the x_{2dk} from available signals.

4. Simulation results

The controlled system is a three phase interleaved boost converter with the parameters listed in Table 2. The experimental bench is described in Fig 5 and is simulated by using MATLAB software. In this respect, all power components, including the FC, are simulated using the relevant Matlab/Simulink power toolbox where current derivative limitation in the FC module is taken into account. Then, the capability of the proposed controller to deal with such limitation will be implicitly illustrated through the different simulation tests (e.g. Figs. 6, 7, 8 14).

4.1. Adaptive controller performances

The proposed adaptive control design is considered with the following numerical values of design parameters which proved to be suitable:

$$k_1 = 400\,,\ \ k_2 = 10^3\,,\ \gamma = 2\times10^{-4} \text{ and } \alpha = 1.2\times10^3\,.$$

These have been selected using the common try-error method that consists in increasing the

parameter values until a satisfactory compromise, between rapidity of responses and control activity, is achieved. The behavior of such a system is illustrated in figures 6 to 8.

a) Regulator sensitivity to load uncertainty

Fig. 6 illustrates the behavior of controlled system with an output voltage reference $V_d = 48V$ (which represents the DC bus voltage) and successive load step changes, the resistance can change between 2.5Ω and 5Ω, yielding variation of 50% of the power of the DC bus. As it can be seen, despite the load resistor uncertainty, the controller behavior is satisfactory. Fig. 6(a) shows a tight voltage regulation under step load changes. Fig. 6(b) shows the change of operation point of the fuel cell voltage, showing its high dependence on the current. Fig. 6(c) depicts the load resistance 50% changes. Fig. 6(d) illustrates the duty cycle variations, including a ripple characteristic of the sliding mode control, also known as chattering [30].

Fig. 7 shows an appropriate current sharing between the interleaved inductor currents for load changes. Figs. 7(a)-(c) depicts the equal current sharing between the modules. Notice that Fig. 7(d) shows the ripple cancellation of the fuel cell current allowed by the interleaved inductor currents.

Fig. 8 illustrates a perfect estimation of uncertain parameter, with negligible steady state error and fast transient response.

Table 2: Parameters of the interleaved boost converter

Parameter	**Symbol**	**Value**
Number of phases	N	3
Inductance value	L	2.2 mH
Inductance ESR	r_L	20$m\Omega$
Output Capacitor	C	1200 μF
Switching frequency	f_s	10 kHz

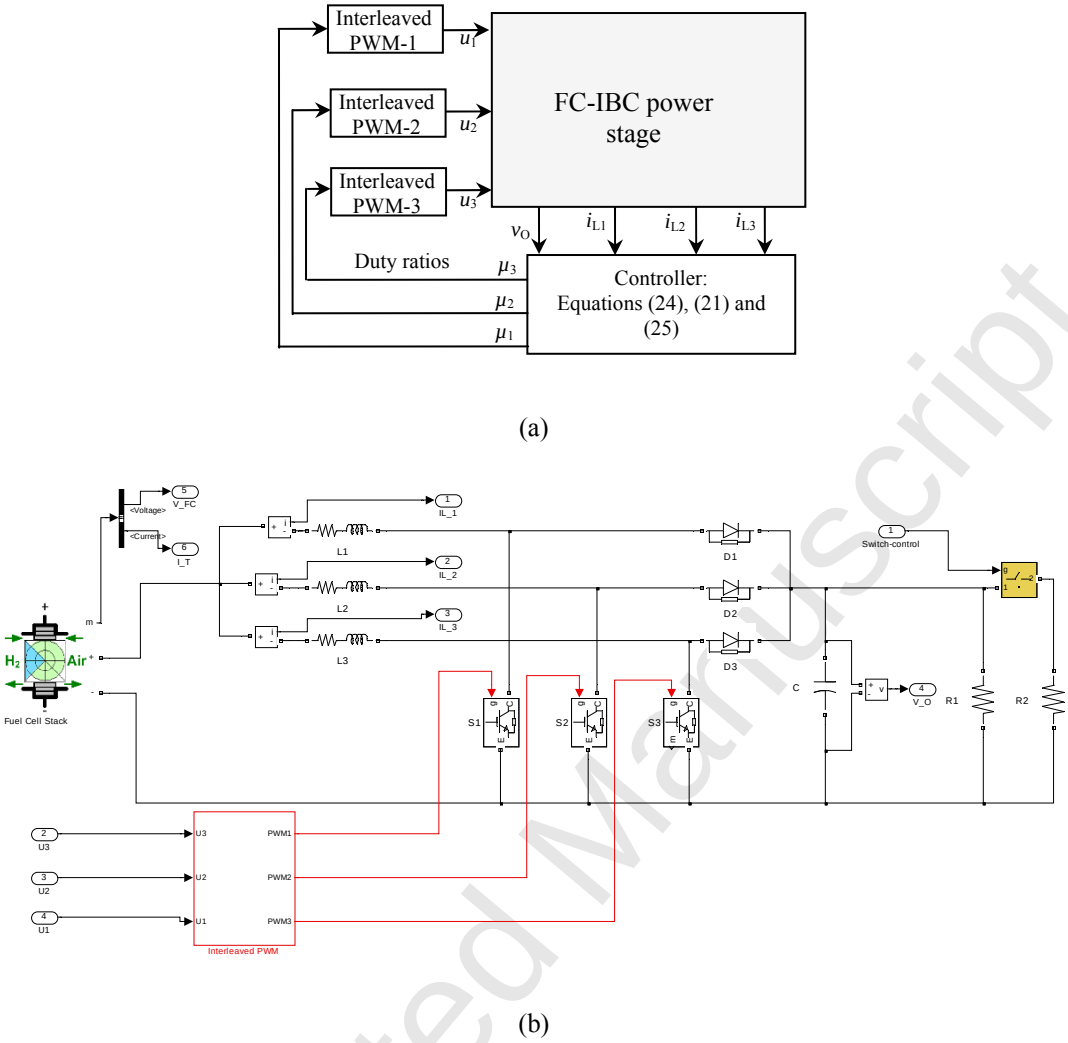

Fig.5: Simulated experimental bench of FC-IBC system: (a) control part; (b) power part.

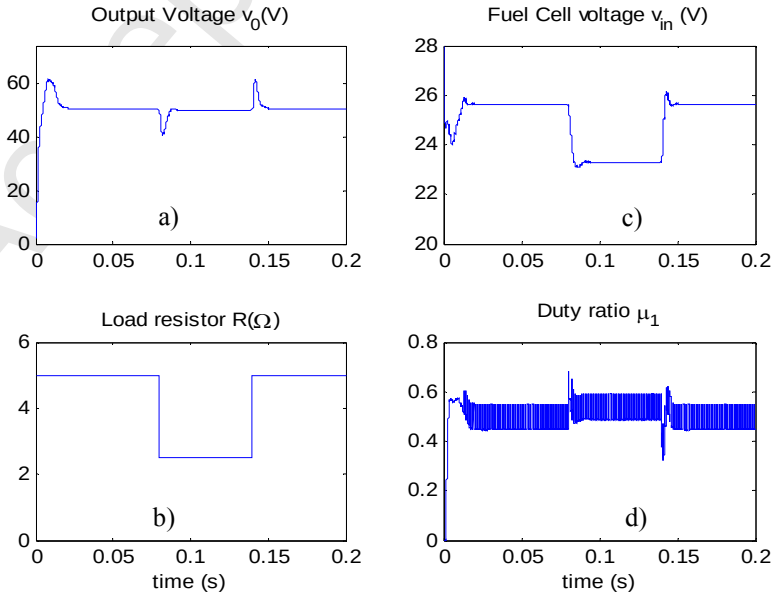

Fig.6: Controller behavior in response to a step reference $V_d = 48V$ and changes in the load resistance

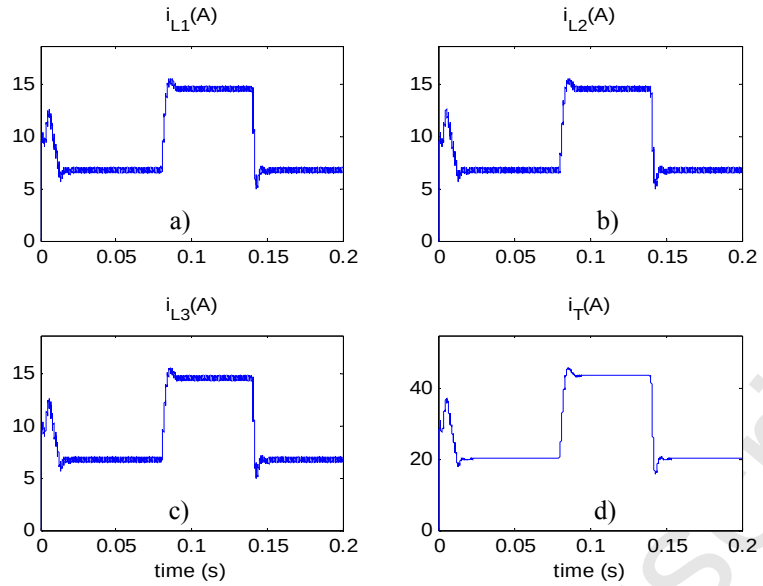

Fig.7: Inductor currents in response to a step reference $V_d = 48V$ and changes in the load resistance

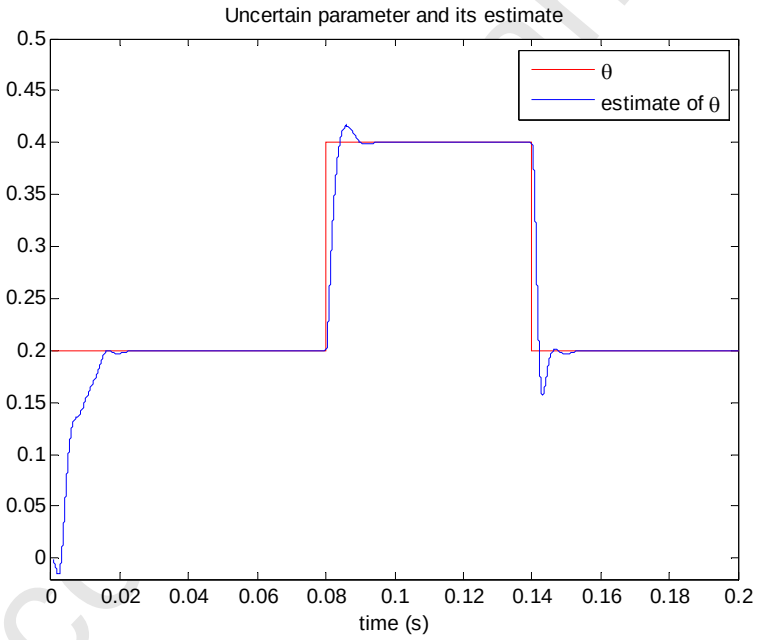

a) Uncertain parameter its estimate

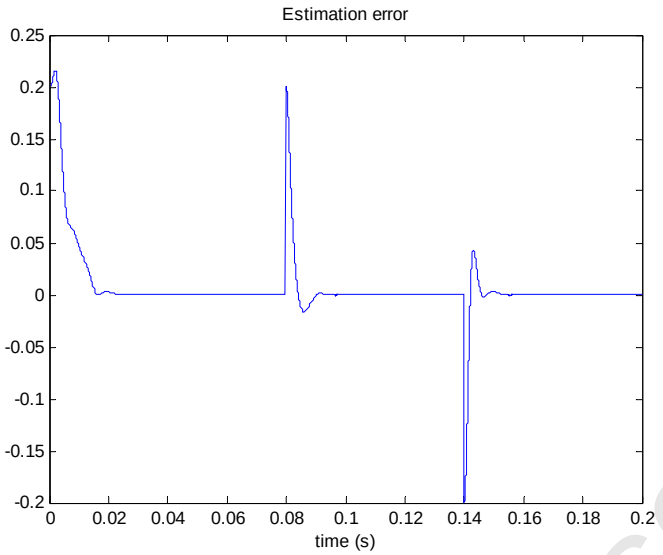

b) Estimation error

Fig.8: Controller estimation performances: a) uncertain parameter and its estimate, b) estimation error

b) Controller behavior in presence of discontinuous conduction mode operation

In practice, dc-dc converters may enter into a discontinuous conduction mode operation. This means that, in each switching period, the current may vanishe during a time interval. The point is that such phenomenon is not accounted for in the control model (4), that is based on in control design. Therefore, it is of interest to check whether the proposed adaptive controller preserves its performances when it faces such converter behavior. To push the converter into discontinuous mode operation, a sudden and drastic change of the load is produced at time instant 0.1*s* (Fig. 9). Then, a drastic decrease of the current is produced that makes the converter operates in discontinuous mode during an interval following the sudden load change. This is illustrated making a zoom on the inductor current during the interval [101.6*ms* 102.4*ms*] (Fig. 10). Fig. 9 shows that the proposed controller is able to face discontinuous mode keeping a tight output voltage regulation. Furthermore, Fig.10 shows that the current sharing requirement, in presence of load changes, is also preserved despite the discontinuous mode.

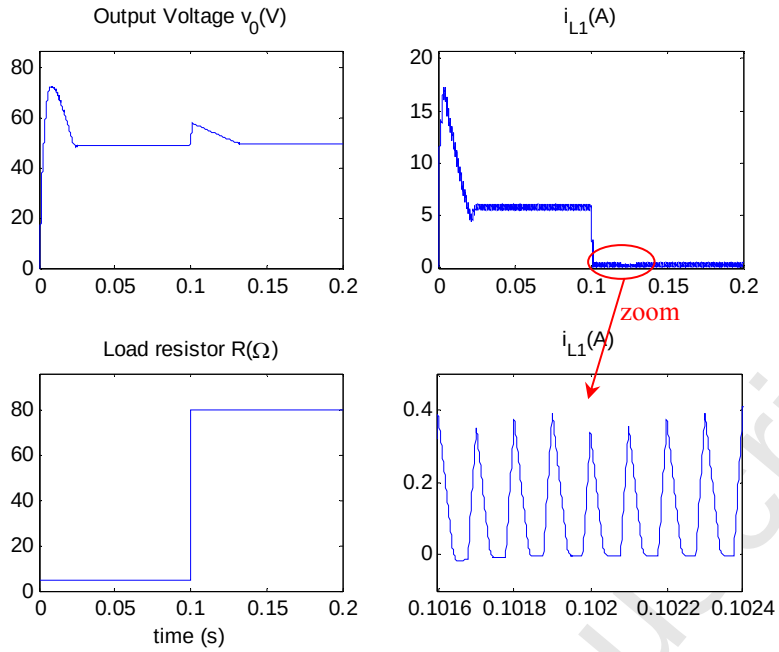

Fig.9: Controller behavior in discontinuous mode

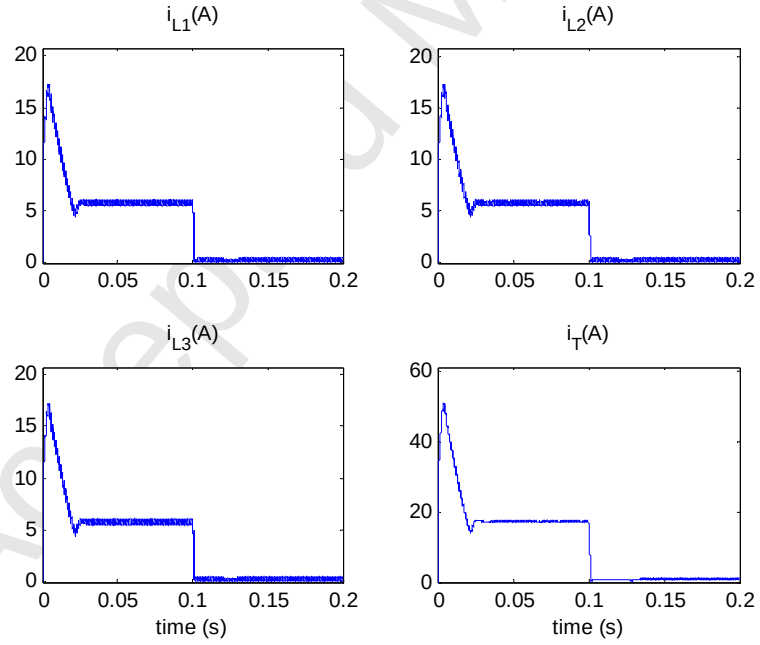

Fig.10: Inductor currents sharing in discontinuous mode

c) Robustness of the controller in presence of fuel cell V-I characterstic uncertainty

Fuel cell is an electrochemical device that directly converts chemical energy to electrical

energy. Its V-I characteristic (known as a polarization curve) may vary even during normal operation conditions, due to changes of air flow rate, supply pressure, temperature, etc. Therefore, it is of interest to evaluate the performances of the proposed adaptive controller in presence of this uncertainty. Fig.12 illustrates the closed-loop behavior in presence of V-I characteristic variations. Specifically, a 10% change is produced on the true V-I characteristic with respect to nominal characteristic. Meanwhile, the controller design is only based on the nominal characteristic (see Fig. 11). The resulting control performances are illustrated by Fig. 12 which shows that output voltage is still well regulated to its desired value $V_d = 48V$. Furthermore, Fig.13 shows the fair current sharing objective is still met.

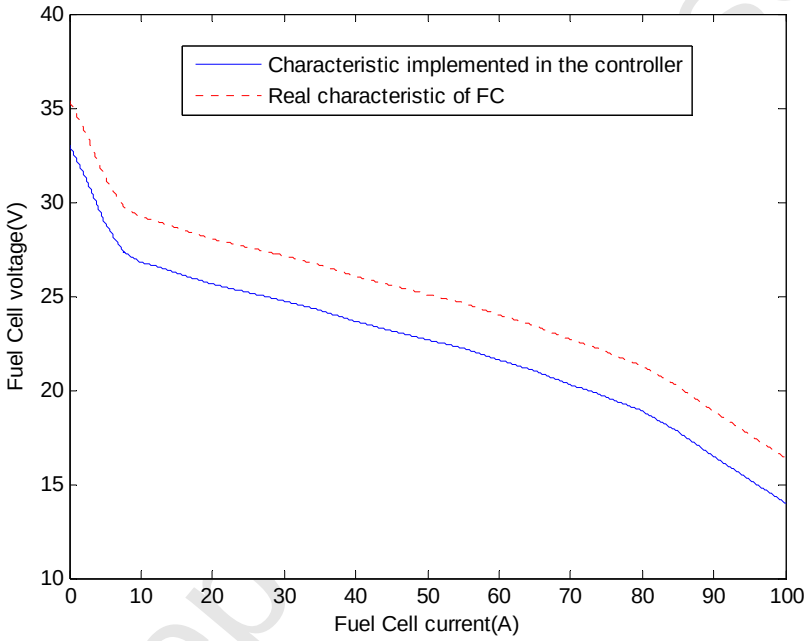

Fig.11: Real V-I characteristic of FC and the implemented one in the controller

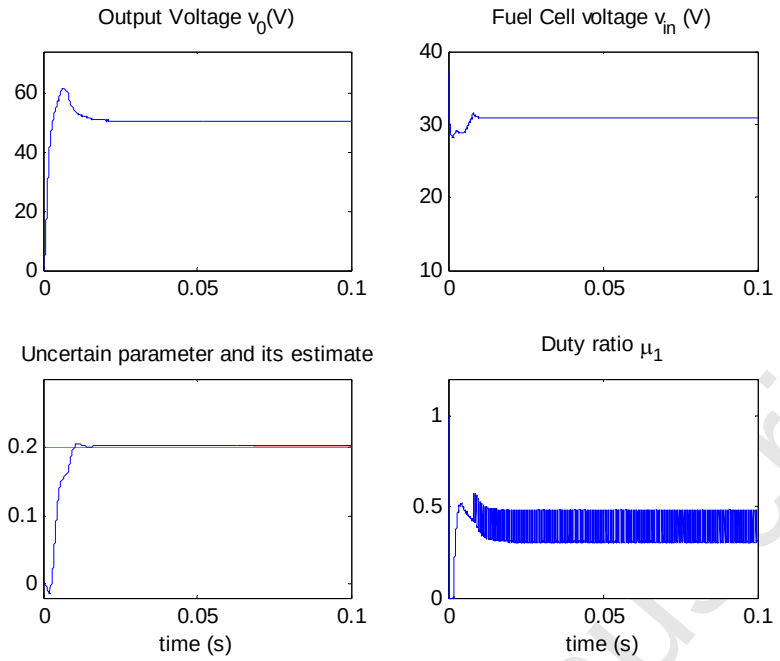

Fig.12: Controller behavior in presence of V-I characteristic uncertainty

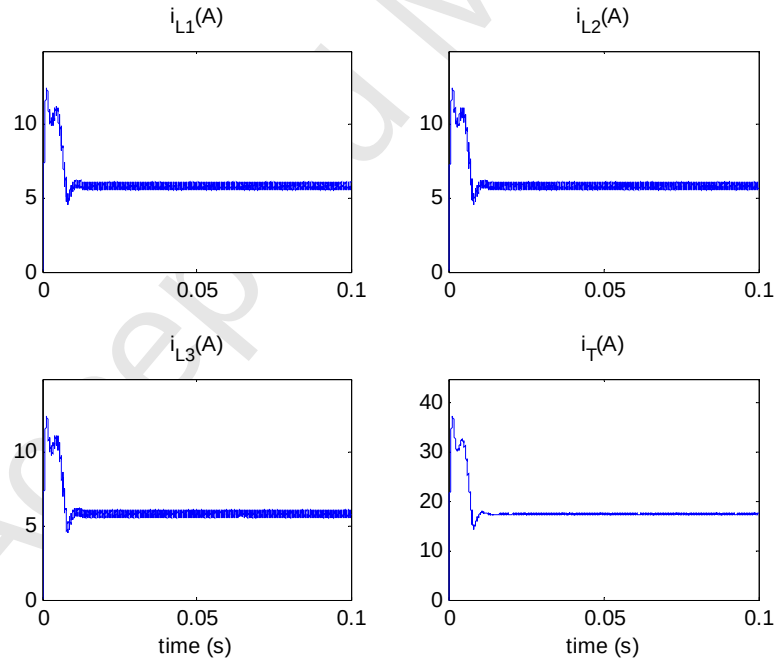

Fig.13: Current sharing in presence of V-I characteristic uncertainty

4.2. Limits of linear controller

To illustrate the supremacy of the proposed nonlinear control strategy over traditional linear

control methods, linear PI regulators are presently considered within the simulated experimental set up of Fig. 14. There PI-1 and PI-2 are PI regulators defined by the usual expressions:

$$C_1(s) = K_1 \frac{(1+T_1 s)}{s} \quad ; \quad C_2(s) = K_2 \frac{(1+T_2 s)}{s} \tag{26}$$

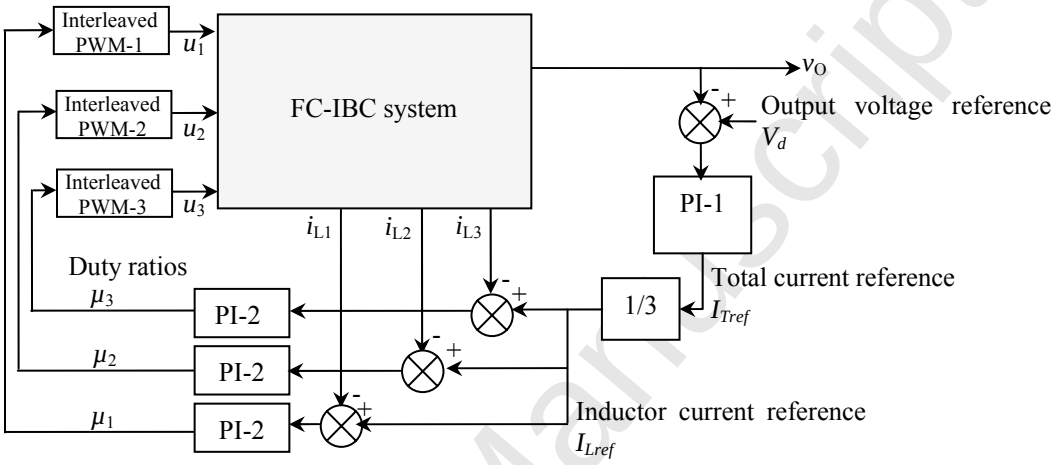

Fig.14. Experimental bench for FC-IBC linear control strategy

In order to design parameters of $C_1(s)$ and $C_2(s)$, a small signal model of the single boost converter is elaborated as shown in Fig. 15.

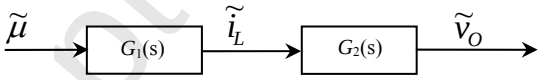

Fig. 15 : Small signal model of boost converter

where:

$$G_1(s) = \frac{\tilde{i}_L}{\tilde{\mu}} = \frac{CV_{On}.s + 2(1-U_n)I_{Ln}}{LC.s^2 + (R_L C + L/R).s + R_L/R_n + (1+U_n)^2} \tag{27}$$

$$G_2(s) = \frac{\tilde{v}_O}{\tilde{i}_L} = \frac{-LI_{Ln}.s - I_{Ln}R_L + V_{On}(1-U_n)}{CV_{On}.s + 2(1-U_n)I_{Ln}} \tag{28}$$

and V_{On} , I_{Ln} , U_n , R_n are the nominal values of v_O , i_L , μ , R, respectively.

Accordingly, the linear control system of Fig. 14 assumes the bloc diagram representation of Fig. 16.

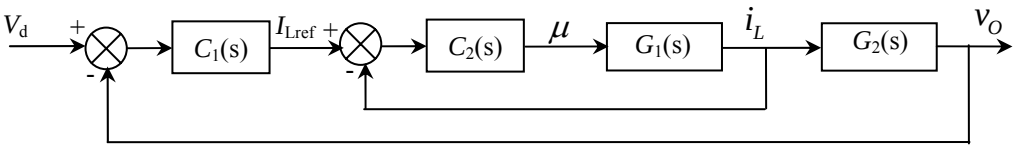

Fig. 16. Closed loop linear control

Presently, the regulators $C_1(s)$ and $C_2(s)$ are tuned using the Sisotool® software integrated in Matlab® (see Fig. 17). Accordingly, the regulators $C_1(s)$ and $C_2(s)$ are optimized in order to satisfy some design requirements such as phase margin (PM), gain margin (GM), settling time. Doing so, the following parameter values have been retained

$$K_1=127.26 \quad ; \quad T_1=0.00017 \quad ; \quad K_2=4.979 \quad ; \quad T_2=0.00037 \tag{29}$$

as they lead to the satisfactory performances, specifically PM=45°, GM=10dB.

The performances of the linear control are illustrated by Fig. 18 and Fig.19. The simulations show clearly that the linear PI-based control strategy performs well as long as the system operates around its nominal operation point, unlike the nonlinear strategy that maintain a high level of performances in all operation conditions, thanks to its adaptation capability. The deterioration of the linear control strategy performances (when the system deviates from its nominal operation point) is presently worsened by the presence of the control input limitation.

The presence of both input limitation [7] and an integrator in the controller make the closed-loop system suffer from what is commonly called ’windup effect'. This means that the system signals are likely to diverge if a disturbance affects the system. Presently, the disturbance is produced by the modeling error resulting from the load resistance uncertainty.

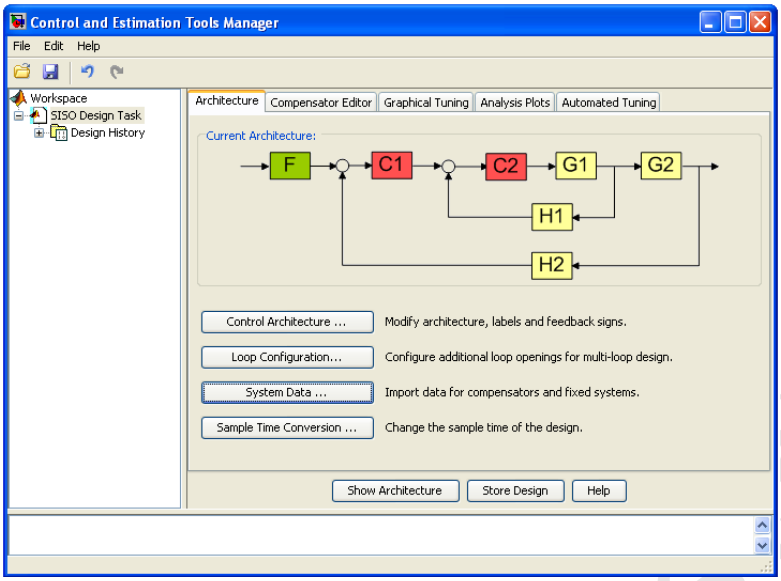

Fig. 17 : Sisotool software of Matlab

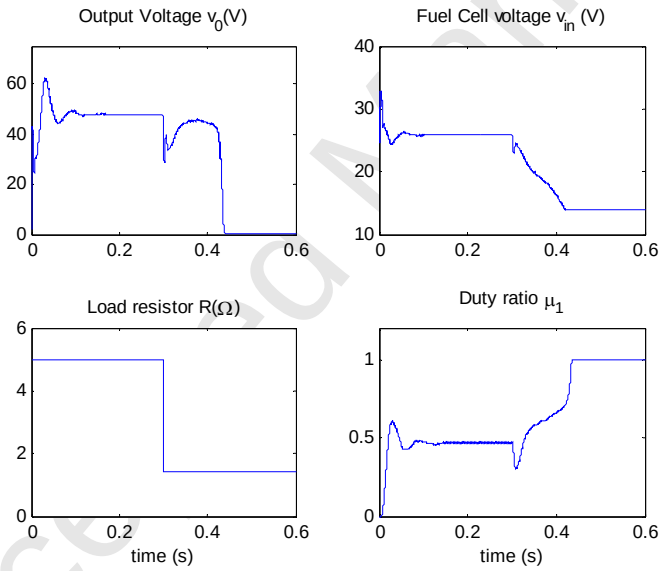

Fig. 18 : Closed loop performances of linear controller

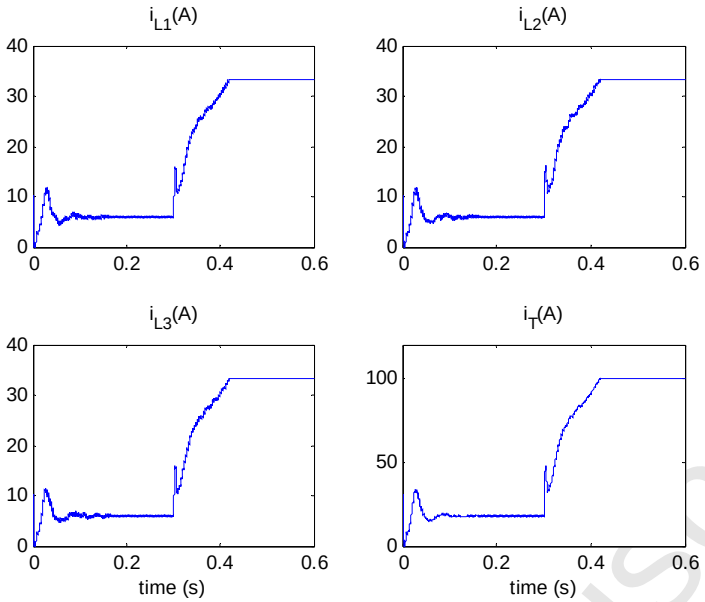

Fig. 19 : Inductor currents with linear controller

5. Conclusion

The problem of controlling a three phase interleaved boost converter associated with fuel cell generation system has been addressed. The control objective is to regulate well the output voltage and ensure a well balanced current sharing between power modules. The control problem complexity comes from the highly nonlinear nature of the FC-IBC association, on the one hand, and load resistance uncertainty and change, on the other hand. The problem is dealt with using an adaptive sliding mode controller, developed on the basis on the system nonlinear model. The adaptive feature is necessary to cope with load resistance uncertainty and change that, presently, simulate variations of the power absorbed in the DC bus. It is formally proved that the proposed adaptive controller meets its control objectives. Furthermore, it is checked using simulations that the controller preserves satisfactory performances in presence of discontinuous modes and FC characteristic changes. Finally, the superiority of the adaptive controller over conventional linear controller is also illustrated by simulation.

6. References

[1] M.F. Akorede, H. Hizam, E. Pouresmail, Distributed energy resources and benefits to environment, Ren. Sust. Energy Rev. 14 (2010) 724-734.

[2] L.H. Chen, J.C. Hwang, S.N. Yeh, G.C. Yu, Analysis and Design of Four-Leg Fuel Cell Boost Converter, in: Proc. of IEEE 32nd Annual Conference on Industrial Electronics (IECON'06), Paris, 2006, pp.4285-4290.

[3] S. Dwari, L. Parsa, A Novel High Efficiency High Power Interleaved Coupled-Inductor Boost DC-DC Converter for Hybrid and Fuel Cell Electric Vehicle, in Proc. of IEEE Vehicle Power and Propulsion Conference (VPPC), Arlington, 2007, pp.399-404.

[4] H. El Fadil, F. Giri, Backstepping Based Control of PWM DC-DC Boost Power Converters, Int. J. Elec. Power Eng. 1(5) (2007) 479-485.

[5] H. El Fadil and F. Giri, Robust and Nonlinear Control of PWM DC-to-DC Boost Power Converters, in: Proc. of the IEEE Power Electronics Specialists Conference (PESC'07), Vigo, 2007, pp. 407-412.

[6] H. El Fadil, F. Giri, Robust nonlinear adaptive control of multiphase synchronous buck power converters, Elsevier Trans. Control Eng. Pract.17(11) (2009) 1245-1254.

[7] H. El Fadil, F. Giri , F.Z. Chaoui, O.El Maguiri, Accounting for Input limitation in Controlling Buck Power Converters, IEEE Trans. Circ. Syst.-I 56(6) (2009) 1260-1271.

[8] H. El Fadil, F. Giri, O. El Maguiri, F.Z. Chaoui, Control of DC-DC power converters in the presence of coil magnetic saturation, Elsevier Trans. Control Eng. Pract. 17(7) 2009 849-862.

[9] H. El Fadil, F. Giri, H. Ouadi, Accounting for coils magnetic saturation in controlling DC-DC power converters, in: Proc. of the IEEE International Conference on Control Applications (CCA'06), Munich, 2006, pp.3163–3168.

[10] C. Gyu-Yeong, K. Hyun-Soo, L. Byoung-Kuk, L.Won-Yong, Design Consideration of Interleaved Converters for Fuel Cell Applications, in: Proc. of International Conference on Electrical Machines and Systems, Seoul, Korea, 2007, pp. 238 – 243.

[11] X. Haiping, E. Qiao, X. Guo, W. Xuhui, L. Kong , Analysis and Design of High Power Interleaved Boost Converters for Fuel Cell Distributed Generation System, in: Proc of 36th IEEE Power Electronics Specialists Conference (PESC'05) , Recife, 2005, pp.140-145.

[12] M. Harinee, V.S. Nagarajan, Dimple, R. Seyezhai, B.L. Mathur, Modeling and design of fuel cell based two phase interleaved boost converter, in: Proc. of IEEE 1st International Conference on Electrical Energy Systems (ICEES), Newport Beach, CA, 2011, pp.72-77.

[13] G. Hoogers, Fuel Cell Technology Handbook, CRC Press, Florida, 2003.

[14] M. Kabalo, B. Blunier, D. Bouquain, A. Miraoui, State-of-the-art of DC-DC converters for fuel cell vehicles, in: Proc. of IEEE Vehicle Power and Propulsion conference (VPPC'10), Lille, 2010, pp.1-6.

[15] A. Khaligh, L. Zhihao, Battery Ultracapacitor Fuel Cell and Hybrid Energy Storage Systems for Electric Hybrid Electric Fuel Cell and Plug-In Hybrid Electric Vehicles: State of the Art, IEEE Trans. Veh. Technol. 58(6) (2010) 2806 - 2814

[16] X. Kong, A.M. Khambadkone, Analysis and Implementation of a High Efficiency, Interleaved Current-Fed Full Bridge Converter for Fuel Cell System, IEEE Trans. Power Electron. 22(2) (2007) 543-550.

[17] P.T. Krein, J. Bentsman , R. M. Bass, B.Lesieutre, On the use of averaging for analysis of power electronic system, IEEE Trans. Power Electron. 5(2) (1990) 182–190.

[18] M. Krstić, I. Kanellakopoulos, P. V. Kokotović, Nonlinear and adaptive control design, John Willy & Sons, NY, 1995.

[19] P.W. Lee, Y. S. Lee, D. K. W Cheng, X. C. Liu, Steady-state analysis of an interleaved boost converter with coupled inductors, IEEE Trans. Ind. Electron. 47(4) (2000) 787-795.

[20] A. Newton, T. C. Green, D. Andrew, AC/DC power factor correction using interleaving boost and Cuk converters, in: Proc. of IEE Power Electronics and Variable Speed Drives Conf., London, 2000, pp. 293-298.

[21] E. Ortjohann, M. Lingemann, A. Mohd, W. Sinsukthavorn, A. Schmelter, N. Hamsic , D. A. Morton, General Architecture for Modular Smart Inverters, in: Proc. of the IEEE International Symposium on Industrial Electronics (ISIE'08), Cambridge, England, 2008, pp. 1525–1530.

[22] N. J. Park, D. S. Hyun, N interleaved boost converter with a novel ZVT cell using a single resonant inductor for high power applications, in: Proc. IEEE conference on Industry Applications, Tampa FL, 2006, pp. 2157–2161.

[23] T. Phatiphat, B. Davat, Study of a multiphase interleaved step-up converter for fuel cell high power applications, Energy Conv. Manag. 51(4) (2010) 826-832.

[24] J.T. Pukrushpan, H. Peng, A.G. Stefanopuolou, Control-oriented modeling and analysis for automotive fuel cell system, J. Dyn. Sys. Meas. Control – Trans. ASME 126 (2004) 14–25.

[25] J.T. Pukrushpan, A.G. Stefanopoulou, H. Peng, Control of Fuel Cell Power Systems: Principles; Modeling; Analysis and Feedback Design, Springer-Verlag, London, 2004.

[26] K. Rajashekara, Hybrid fuel-cell strategies for clean power generation, IEEE Trans. Ind. Appl. 41(2005) 682 – 689.

[27] H. B. Shin, J. G. Park, S. K. Chung, H. W. Lee, T. A. Lipo, Generalised steady-state analysis of multiphase interleaved boost converter with coupled inductors, IEE Trans. Elec. Power Appl. 152(3) (2005) 584-594.

[28] J.-J. E. Slotine, W. Li, Applied nonlinear control, Prentice Hall, Englewood Cliffs, NJ, 1991.

[29] P. Thounthong, P. Sethakul, S. Rael, B. Davat, Design and implementation of 2-phase interleaved boost converter for fuel cell power source, in: Proc. of 4th IET Conference on Power Electronics Machines and Drives (PEMD), York, 2008, pp.91-95.

[30] V.I. Utkin, Sliding Modes and Their Application in Variable Structure Systems, MIR, Moscow, 1978.

[31] M. Veerachary, T. Senjyu, K. Uezato, Maximum power point tracking of coupled inductor interleaved boost converter supplied PV system, IEE Trans. Electr. Power Appl. 150 (2003) 71-80.

[32] X. Yu, M.R. Starke, L.M. Tolbert, B. Ozpineci, Fuel cell power conditioning for electric power applications: a summary, IET Trans. Elec. Power Appl. 1(5) (2007) 643–656.

[33] M. T. Zhang, M. M. Jovanovic, F. C. Lee, Analysis and evaluation of interleaving techniques in forward converters, IEEE Trans. Power Electron. 13(4) (1998) 690–698.